Isı Bilimi ve Tekniği Dergisi, 43, 2, 233-242, 2023
J. of Thermal Science and Technology

ISSN 1300-3615
e-ISSN 2667-7725
https://doi.org/10.47480/isibted.1391729

NUMERICAL ANALYSIS AND DIFFUSER VANE SHAPE OPTIMIZATION OF A RADIAL COMPRESSOR WITH THE OPEN-SOURCE SOFTWARE SU2

Mustafa Kürşat UZUNER*, Altuğ Melik BAŞOL, Bob MISCHO***, Philipp JENNY******
*Özyeğin University Graduate School of Science and Engineering, Cekmekoy, Istanbul, Türkiye
kursat.uzuner@ozu.edu.tr, ORCID: 0000-0003-2880-7300
**Özyeğin University Graduate School of Science and Engineering, Cekmekoy, Istanbul, Türkiye
altug.basol@ozyegin.edu.tr, ORCID: 0000-0002-7289-7246
***MAN Energy Solutions Schweiz AG, Zurich, Switzerland, bob.mischo@man-es.com
****MAN Energy Solutions Schweiz AG, Zurich, Switzerland, philipp.jenny@man-es.com, ORCID: 0009-0005-8770-8689

(Geliş Tarihi: 19.06.2023, Kabul Tarihi: 30.10.2023)

Abstract: In recent years, the usage of open-source computational fluid dynamics tools is on a rise both in industry and academia. SU2 is one of these open-source tools. Unlike other open-source alternatives, SU2 is equipped with boundary condition types, solvers and methods that are especially developed for the analysis and design of turbomachinery. The aim of this work is to explore and investigate the capabilities of SU2 in the prediction of performance parameters of radial compressors. Two different single stage shrouded compressor geometries, one with a vaneless diffuser and the other with a vaned diffuser have been investigated with steady state CFD. The compressors were designed by MAN Energy Solutions Schweiz AG. Computational results with SU2 showed a satisfactory agreement with both the experimental data and reference CFD solutions obtained with Fidelity Flow, which is formerly known as Numeca Fine TURBO. Only at the relatively higher mass flow rates the difference between references and SU2 were higher compared to other operating points. After performance parameters were successfully calculated with SU2, the optimization tools that come with SU2 were also used. A 2D adjoint optimization study on the vane of the vaned diffuser was carried out. The study was carried out at a single operating point that is close to choke conditions. The loss generated by the large separated flow region at the suction side of the diffuser vane was reduced by 0.55 % in the optimized geometry using minimal modifications on the existing vane geometry to keep the performance of the compressor intact at other operating points. However, the resulting modification increased the total pressure loss by 0.86 % at one of the design operating points. This performance penalty could be due to the discontinuity in the vane geometry generated by the optimizer. Overall, the study shows that SU2 has the basic numerical schemes and models that are required for the analysis of radial turbomachinery flows and geometry optimization.
Keywords: Computational Fluid Dynamics, Open-source, SU2, Turbomachinery, Compressor, Optimization

AÇIK KAYNAK AKIŞKANLAR DİNAMİĞİ YAZILIMI SU2 İLE RADYAL BİR KOMPRESÖRÜN PERFORMANS ANALİZİ VE OPTİMİZASYONU

Özet: Son yıllarda açık-kaynak hesaplamalı akışkanlar dinamiği yazılımlarının kullanımı hem akademi hem de endüstride gittikçe yaygınlaşmaktadır. SU2, bu açık kaynak akışkanlar dinamiği araçlarından biridir. Diğer açık kaynak araçlarda görülmeyen turbomakine simülasyonu ve tasarımına özel sınır koşulları, çözücüler ve metotlar SU2 içerisinde mevcuttur. Bu çalışmanın amacı, bir radyal kompresörün performans parametrelerinin SU2 ile belirlenmeye çalışılarak SU2'nin kabiliyetlerinin incelenmesidir. Bunun için tek aşamalı, kanatçıklı ve kanatçıksız difüzörlü olmak üzere iki farklı radyal kompresör kullanılmıştır. Bu kompresörler MAN Energy Solutions Schweiz AG tarafından tasarlanmıştır. SU2, deneysel veriler ve Fidelity Flow ile elde edilen sonuçlarla kıyaslandığında yeterli benzerlikte sonuçlar vermiştir. Yalnızca yüksek debili çalışma koşullarında referanslar ile aradaki farkın diğer noktalara göre açıldığı gözlemlenmiştir. Performans parametrelerinde başarılı sonuçlar elde edildikten sonra SU2 içerisinde hazır olarak bulunan optimizasyon araçlarının kabiliyetleri de denenmiştir. Kanatçıklı difüzörün kanatçığı üzerinde iki boyutlu bir adjoint optimizasyon yapılarak optimizasyon kabiliyetleri incelenmiştir. En kötü performansın görüldüğü, boğulma koşullarına yakın bir çalışma noktası optimizasyon için seçilmiştir. Optimizasyon sırasındaki şekil bozunumları başka çalışma noktalarında performansı aynı tutabilmek için olabildiğince küçük tutulmuştur. Kanatçığın basınç tarafında görülen akım ayrılmasının sebep olduğu kayıp optimizasyon sonucu %0.55 azaltılmıştır. Ancak, optimize edilmiş kanatçık profili bir

başka tasarım çalışma noktasında denendiğinde toplam basınçta görülen kaybın %0.86 arttığı gözlemlenmiştir. Bu performans kaybının muhtemel ana sebebi olarak optimizasyon sonucu kanatçıkta oluşan kesiklilik gösterilebilir. Genel olarak bu çalışma, SU2'nin radyal turbomakine analizi ve optimizasyonu için gerekli temel nümerik şemalara ve modellere sahip olduğunu göstermektedir.
Anahtar Kelimler: Hesaplamalı Akışkanlar Dinamiği, Açık Kaynak, SU2, Turbomakine, Kompresör, Optimizasyon

NOMENCLATURE

Polytropic Efficiency (Total to Total)	$\eta = \frac{R}{cp}\frac{\log\left(\frac{P_{t_5}}{P_{t_1}}\right)}{\log\left(\frac{T_{t_5}}{T_{t_1}}\right)}$ (1: Inlet) (5: Outlet)
Work Input Coefficient [-]	$\mu_0 = \Delta h_{t_{1-5}}/u_2^2$
Pressure Rise Coefficient [-]	$\mu_y = \eta\mu_0$
Volume Flow Coefficient [-]	$\Phi = \frac{\dot{m}}{\rho_{t_1} u_2 D_2^2}$
Gas Constant $\left[\frac{J}{kgK}\right]$	$R = 287.4$
Heat Capacity $\left[\frac{J}{kgK}\right]$	$cp = 1006$
Impeller Tip Rotational Speed $[\frac{m}{s}]$	$u_2 = \frac{D_2\omega}{2}$
Impeller Tip Diameter [m]	D_2
Mass Flow Rate $\left[\frac{kg}{s}\right]$	$\dot{m}$
Total Density at Inlet Conditions $\left[\frac{kg}{m^3}\right]$	ρ_{t_1}
Rotational Speed $\left[\frac{rad}{s}\right]$	ω
Total Pressure $[Pa]$	P_t
Total Temperature $[K]$	T_t
Total Enthalpy Difference $\left[\frac{J}{kg}\right]$	Δh_t

Total values are calculated by area averaging.

INTRODUCTION

Computational Fluid Dynamics (CFD) plays a key role in the design of turbomachinery. Even though there are a variety of commercial codes that serve the needs of the designers, open source CFD tools have started to gain attention in recent years. However, most of the open source CFD tools are built for general purpose applications and do not contain turbomachinery specific features. The open-source flow simulation and design software SU2 is different in that sense. It is equipped with turbomachinery specific features such as nonreflecting boundary conditions and special mesh interfaces. In open literature, several contributions on turbomachinery analysis conducted with SU2, are available. A very similar work, which performs an analysis of a centrifugal compressor with vaneless diffuser shows the predictive capability of SU2 when compared to ANSYS and experimental data (de Castro, 2019). An important output of this work is related to the mesh topology dependency of SU2. Different grid topologies, namely C-grid and O-grid, are tested, and SU2 is found out to be working better with O-grid topology when a second order accurate solution is desired. Another example where turbomachinery capabilities of SU2 are compared to experimental data and ANSYS-CFX is also available (Yan *et.al,* 2023). The single passage steady, full-annulus unsteady and aeroelasticity capabilities of SU2 are investigated on NASA Stage 35, TUDa-GLR-OpenStage, and a linear cascade SC1. Results are compared with ANSYS-CFX and experimental data. Overall, SU2 showed satisfactory agreement in these comparisons up to near-stall operating points. Additionally, an analysis of a one-and-a half stage, stator-rotor-stator, axial turbomachinery (Mollá, 2017), and an analysis of a simple radial inflow turbine (Keep *et.al,* 2017) are also performed with SU2. These works mostly incorporate mixing-plane and non-reflecting boundary condition features with periodic boundary faces (Giles, 1990). SU2 can also be utilized for design purposes as well with its simple 2D capabilities (de Koning, 2015). Additionally, it can be used with its built-in optimization tools for design (Vitale *et.al,* 2020) and use special features such as harmonic balance as well (Rubino *et.al,* 2020).

Adjoint methods are commonly used for optimization in computational fluid dynamics and has been pioneered by Jameson in the aerospace field (Giles and Pierce, 2000). Adjoint equations are derived from the governing equations and the sequence of discretization change the type of adjoint method. There are two adjoint methods, continuous and discrete. For continuous adjoint, adjoint equations are formulated before the governing equations are discretized, and for discrete adjoint, adjoint equations are formulated after the governing equations are discretized (Ntanakas and Meyer, 2014). In terms of turbomachinery optimization, the use of adjoint methods is widely seen as well. A gradient based shape optimization of NASA Rotor 37 can be found where the shock related tonal noise is minimized when maximizing the isentropic efficiency (Katsapoxaki *et.al,* 2023). Moreover, the SRV2 radial compressor is optimized to increase the total-to-total efficiency at highest efficiency meanwhile conserving its wide operating range (Châtel *et.al,* 2022). Optimization is conducted with a gradient-based method, where gradients are found with the adjoint approach. Another optimization study on SRV2-O compressor is present where the volute designed for this compressor is optimized using adjoint optimization (Hottois *et.al,* 2023). Other studies where turbomachinery targeted optimization method developments are also

available. A new volumetric parametrization approach for gradient-based shape optimization focused on turbomachinery stages is introduced, where the need for an extra mesh deformation tool is eliminated (Trompoukis *et.al,* 2023). In another study, the robustness of the optimized design is aimed to be improved by considering the effect of uncertainties with a Surrogate-Assisted Gradient-Based (SAGB) optimization method (Luo *et.al,* 2022). Additionally, a multi-row discrete adjoint solver development combining manual and automatic differentiation is also available (Wu *et.al,* 2023).

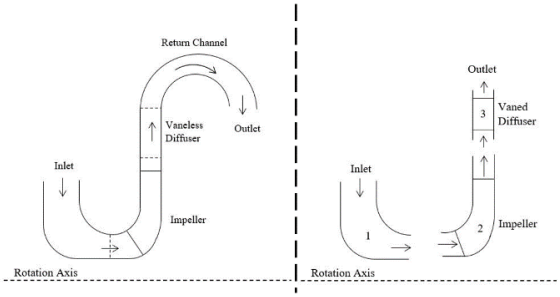

Figure 1. Compressor Flow Paths for each Case

SU2 has its own Adjoint Optimization tool integrated in the package, and both continuous and discrete methods are available. There are two shape deformation methods used in SU2, which are Hicks-Henne (Hicks and Henne, 1978) and FFD (Free Form Deformation) (Koshakji *et.al,* 2013) methods. Both methods work by changing the design variables to see how the changed geometries would perform. FFD deforms a specified space around the object interested whereas other methods deform the geometry directly (Koshakji *et.al,* 2013). Hicks-Henne deformation method is only available with 2D cases whereas FFD is applicable to both 2D and 3D cases.

However, a detailed investigation of the SU2's flow analysis capabilities, the computational cost of its solvers and their parallel scalability against other proven commercial codes is still needed to identify regions for further improvements. In the first part of this study, the capabilities of the solvers in SU2 are tested on two single stage radial compressor geometries, one with a vaneless and the other with a vaned diffuser. The compressor stages used in this work are proprietary designs of MAN Energy Solutions Schweiz AG. The company provided experimental and reference CFD data obtained with 'Fidelity Flow' for comparison with the SU2 results. In the second part of this study the shape optimization capabilities of SU2 are evaluated. In this regard, the existing compressor vane geometry from the vaned diffuser case is considered as the baseline design, and it is optimized using the adjoint optimization tools in SU2 in 2D. The performance improvements is compared to the baseline design.

NUMERICAL METHODOLOGY

Two different single stage radial compressor geometries have been considered. Schematics of the meridional flow paths of the compressors are shown in Figure 2. Both compressors contain shrouded impellers. One of the geometries, Case1, included a vaneless and the other one, Case2, was equipped with a vaned diffuser. The meshes were generated using 'Fidelity Automesh Autogrid'.

The zones (inlet-impeller-diffuser) of the compressor in Case 2 are meshed separately. In all meshes a multi-block structured O-grid mesh topology was utilized. A close view of the mesh around the impeller are shown in Figure 2 and Figure 3.

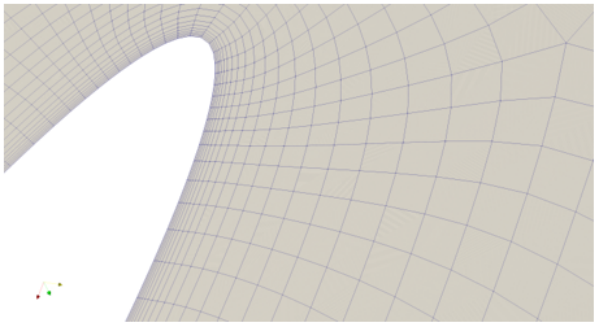

Figure 2. Close-up View of Impeller Leading Edge Mesh

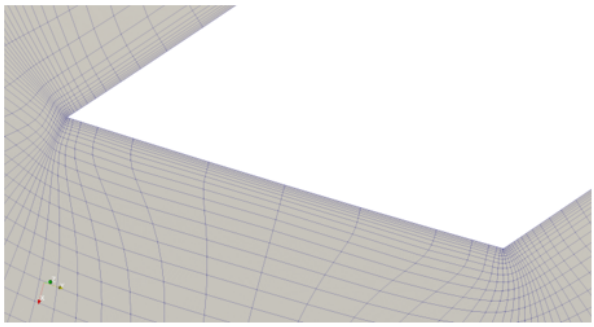

Figure 3. Close-up View of Impeller Trailing Edge Mesh

The different mesh zones in Case 2 are solved in either stationary or rotating frame of references. The interfaces between the different mesh zones were treated with the mixing plane interface condition. At the inlet zone a uniform total pressure, total temperature and flow directions were specified as inlet boundary conditions. At the diffuser zone outlet, averaged static pressure at the outlet was applied. At the walls, no slip boundary conditions were defined. At the periodic faces, periodic boundary conditions were specified.

The compressor in Case 1 was meshed as a single zone. Due to the vaneless diffuser, the entire domain could be run in rotating frame of reference. So, no interface treatment was necessary in Case 1. Apart from that, same type boundary conditions were specified at the domain boundaries as in Case 2.

For the closure of the RANS equations, different turbulence models are available in SU2. In this study, k-omega SST (Menter, 1994) turbulence model was used.

SU2 offers different schemes for the discretization of the RANS equations. In this study, Backward Euler scheme was used for the temporal discretization. The implicit character of the scheme enables to use relatively large time steps compared to explicit schemes and offers a superior convergence behavior compared to explicit schemes. For the spatial discretization first and second order Roe schemes are available in SU2. However, second order scheme led to numerical instability at the cutback impeller trailing edge. Local mesh refinement at the trailing edge region could also not resolve the numerical instability and therefore the first order accurate Roe scheme was used in all the computations. Air, modeled as perfect gas, was used as the working fluid. For convergence, the mass imbalance between the inlet and outlet were monitored, and simulations with imbalance less than 0.5% is assumed to be converged.

To determine the required mesh resolution for a grid insensitive solution a mesh dependency study was carried out. The mesh dependency study was carried out only for Case 2. Accordingly, three different meshes were generated. Statistics of the meshes used in the study are given in Table 1.

Table 1. Total Number of Cells used in the generated grids.

Mesh 1	Mesh 2	Mesh 3
0.4m	1.6m	3.9m

Mesh dependency study is done by comparing the total enthalpy difference, Δh_{tot}, and flow coefficient, Φ, by taking the corresponding values from experiment as the reference. The percent changes for Δh_{tot} and Φ as the mesh cell count increases are considered. As it can be seen from Figure 4 and Figure 5, the difference between Mesh 1 and Mesh 2 is higher compared to Mesh 2 and Mesh 3. The percent changes for Δh_{tot} and Φ are 3.77 and 2.68 as the mesh changes from Mesh 1 to Mesh 2, and 0.98 and 0.4 as the mesh changes from Mesh 2 to Mesh 3, respectively. Therefore, since the changes from Mesh 2 to Mesh 3 are below 1%, Mesh 2 is determined to have the required resolution for capturing the necessary flow characteristics.

For the geometry with the vaneless diffuser, same mesh settings with Mesh 2 are incorporated. Therefore, a separate mesh dependency study for the vaneless diffuser geometry is not conducted. For the optimization study, the same mesh settings are applied to the 2D diffuser vane blade.

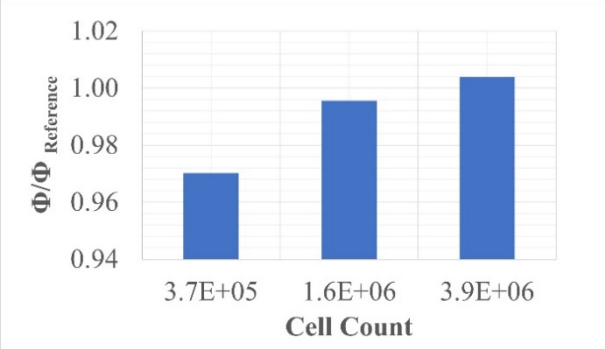

Figure 4. Change of Flow Coefficient with respect to Cell Count

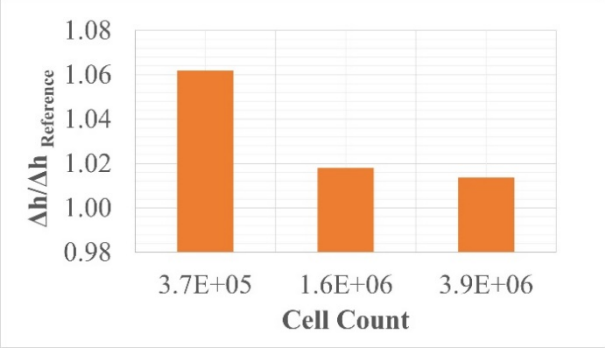

Figure 5. Change of Enthalpy Difference Between Inlet and Outlet with respect to Cell Count

RESULTS

Both compressor geometries Case 1 and 2 were solved at a single rotational speed and at constant total conditions at the inlet boundary. However, the static pressure at the diffuser outlet were varied to evaluate the performance of the compressor at different mass flow rates.

Operating points close to the stall condition could not be simulated precisely because SU2 is not equipped with an outlet boundary condition type that allows to impose mass flow rate, which is a shortcoming for turbomachinery flow simulations. For flat compressor characteristics close to the stability limit, ability to specify outlet mass flow rate as boundary condition is a necessity. When the static pressure is imposed at the outlet boundary, numerical/physical pressure oscillations eventually lead to strong mass flow fluctuations and no fixed stable operating point may be found.

For two operating points, one with low and one with high polytopic efficiency, flow fields are compared between SU2 and 'Fidelity Flow'. With 'Fidelity Flow', a second order central spatial scheme with a Jameson type dissipation and an explicit q-stage Runge-Kutta local time stepping scheme was used. Since SU2 was only able to work with a first order scheme, the difference between these solvers is very apparent in the flow field comparison. The comparison stations are chosen from diffuser zone as shown in Figure 6.

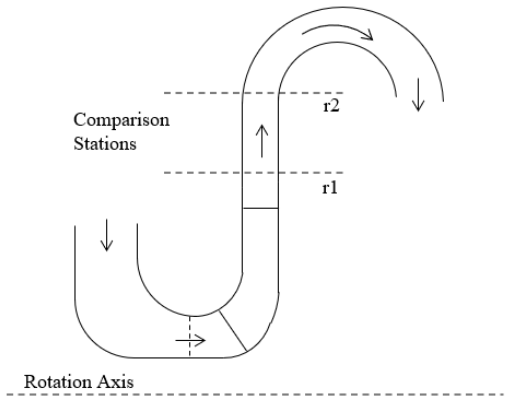

Figure 6. Stations in Case 1 for Flow Field Comparison

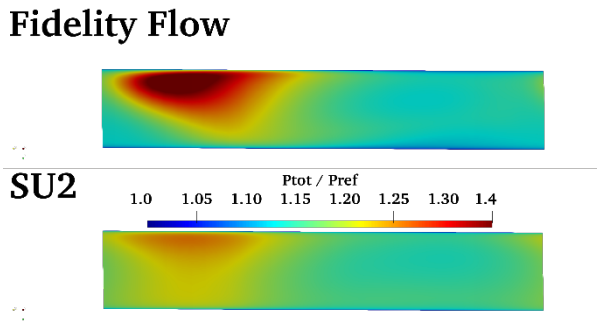

Figure 7. Total Pressure Comparison at Station r1 for Low η

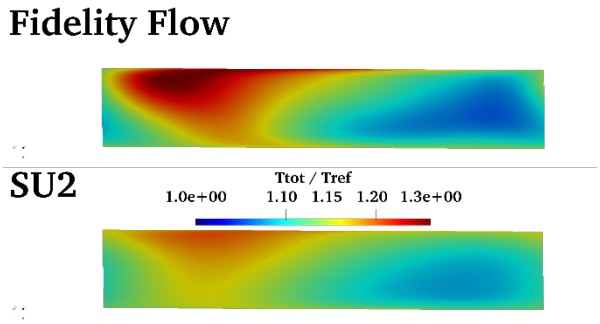

Figure 8. Total Temp. Comparison at Station r1 for Low η

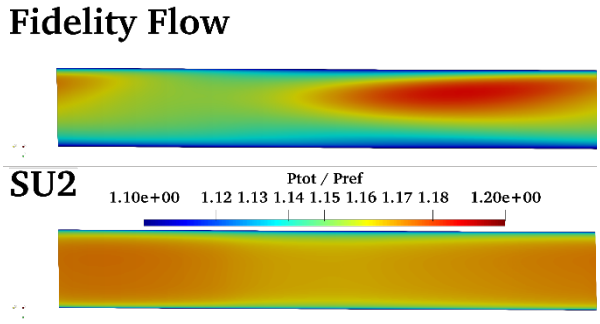

Figure 9. Total Pressure Comparison at Station r2 for Low η

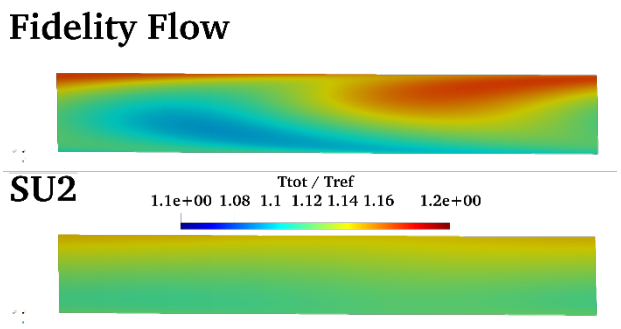

Figure 10. Total Tempe. Comparison at Station r2 for Low η

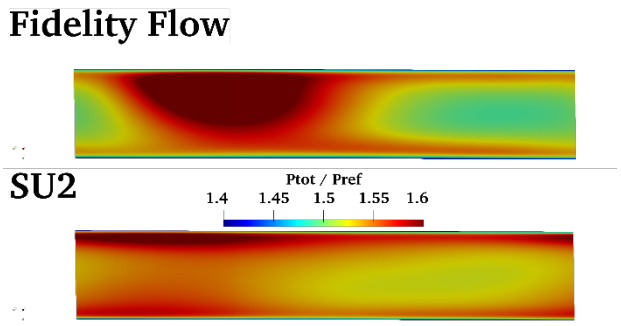

Figure 11. Total Pressure Comp. at Station r1 for High η

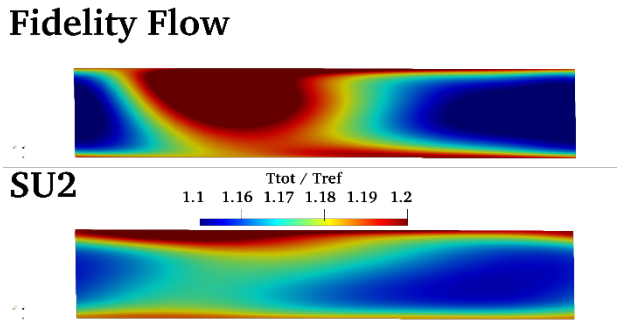

Figure 12. Total Temp. Comparison at Station r1 for High η

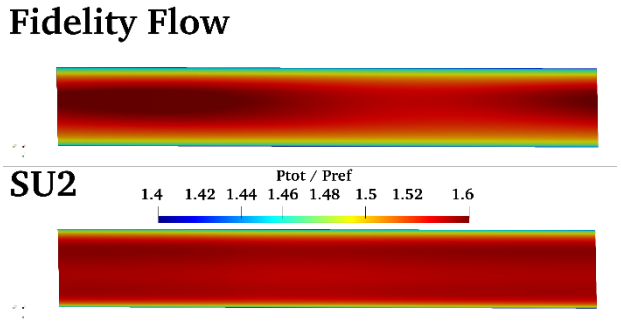

Figure 13. Total Pressure Comparison at Station r2 for High η

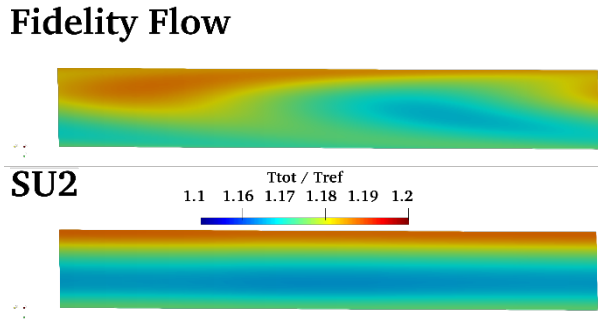

Figure 14. Total Temp. Comparison at Station r2 for High η

Even though the integral parameters such as efficiency do not change significantly, the differences between using a lower and higher order spatial discretization scheme are visible in the flow field contours shown in between Figure 7 and Figure 14. Trailing edge of the impeller corresponds to middle of these contours. As it can be seen from these figures, SU2 shows a much significant diffusion in terms of flow structures as the flow travels from r1 to r2. Even though SU2 captures some of the flow structures it is not as good as 'Fidelity Flow' results. This is an expected behavior since SU2 results are obtained by using a first order spatial scheme, whereas 'Fidelity Flow' results are obtained by using a second order spatial scheme.

Figure 15 and Figure 16 show the comparison of SU2 results with Fidelity Flow results and experimental data for Case 1. As shown in Figure 15, SU2 predicts the outlet pressure of the compressor very close to Fidelity Flow results. In Figure 16, other performance parameters of the compressor such as polytropic efficiency, work input coefficient and pressure rise coefficients are compared between the different solvers and experimental data. Both CFD and experimental data are taken from values obtained at the inlet and outlet plane of the vaneless diffuser. The definitions of the parameters are given in the nomenclature. Here, one can also observe that the predictions of SU2 agree well with 'Fidelity Flow' results. When compared with the experimental data SU2 shows comparable results. The agreement between SU2 results and experimental data for pressure rise coefficient is better compared to polytopic efficiency and work input coefficient. This is due to not including cavity flows in the CFD model to keep the model simple. Cavity flows would induce higher losses, which is why in experimental data efficiency is lower and work input coefficient is higher compared to CFD results. Because of this, the difference between experimental data and CFD results are somewhat compensated for pressure rise coefficient and are much more similar.

All the operating points given in Figure 15 and Figure 16 showed similar convergence characteristics with SU2. Overall SU2 would need around 2000 to 2500 iterations to reach a converged solution. Convergence was checked by using the mass flow rates at the inlet and outlet.

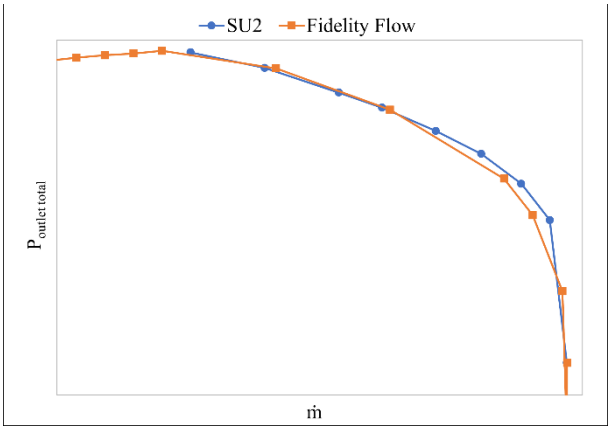

Figure 15. Outlet P_{total} vs ṁ for Case 1

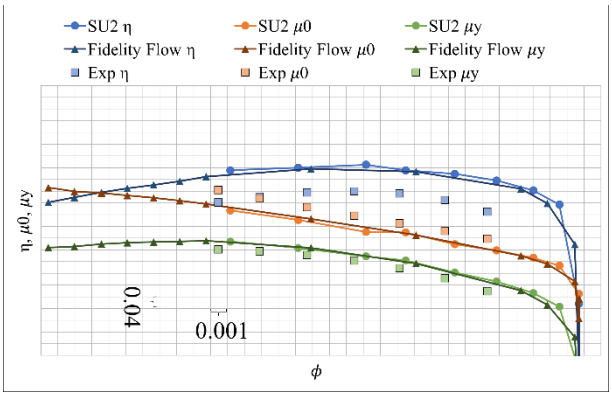

Figure 16. η, μ_0 and μ_y vs ϕ for Case 1

Next, the performance parameters of Case 2 predicted with SU2 are compared with 'Fidelity Flow' results. As shown in Figure 17 and Figure 18, one can say that there is a satisfactory match between the two CFD solutions. However, the agreement between the two solutions is relatively lower compared to Case 1. In Figure 18, SU2 shows good accuracy for the most part when compared to 'Fidelity Flow' result. A similar issue that was apparent in Case 1 when comparing the experimental data and CFD results can also be seen here as well. For efficiency, SU2 and Fidelity Flow results agree more compared to work input and pressure rise coefficients. The difference at work input coefficient indicates that SU2 underpredicts losses compared to 'Fidelity Flow'. This difference then transferred on to pressure rise coefficient since all these parameters are linked together.

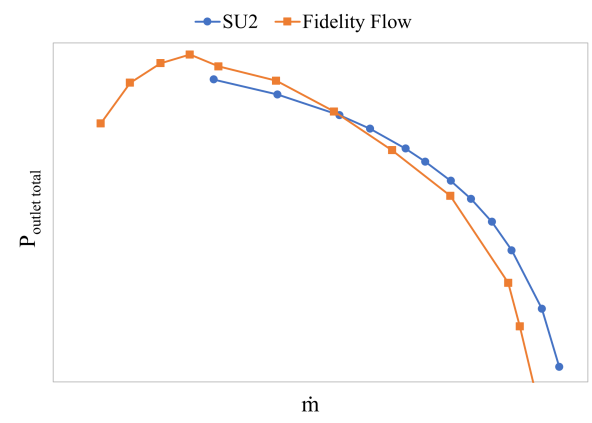

Figure 17. Outlet P_{total} vs $\dot{m}$ for Case 2

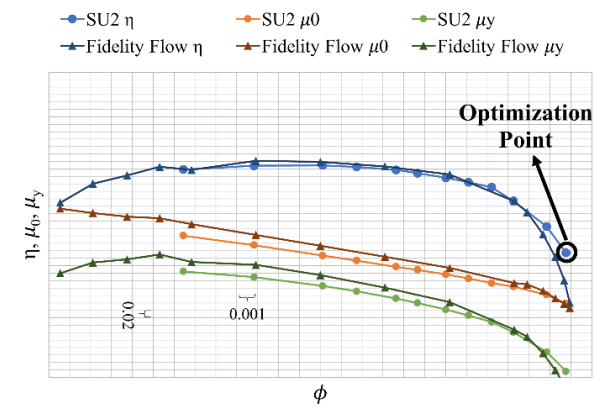

Figure 18. η, μ_0 and μ_y vs ϕ for Case 2

DIFFUSER VANE SHAPE OPTIMIZATION

The geometry of the vane in the vaned diffuser case is prismatic, which means that the profile of the diffuser blade does not change in spanwise direction, so it is possible to follow a 2D modelling approach. The flow field comparison around diffuser vane is shown in Figure 19. As it can be seen from Figure 19, flow field section taken from 3D solution at the mid span of the vane and 2D flow field solution are very similar. Therefore, the optimization of the diffuser vane is done in 2D. Since FFD has a broader applicability and great potential in a possible future 3D case, FFD method is used as the deformation method.

At the operating condition with the worst polytropic efficiency, there is a separation region that cover a considerable portion of the diffuser vane blade suction side, which is shown in Figure 20. This separated flow region is selected for the optimization problem with the aim of reducing the pressure loss at the diffuser for that operating condition.

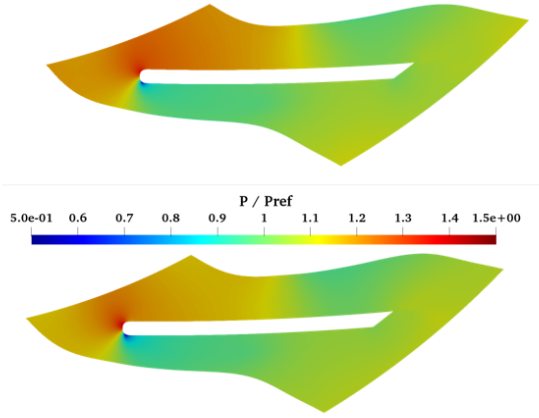

Figure 19. Mid-span Section of 3D Solution (Top) and 2D Solution (Bottom) Flow Field Comparison

For objective and constraint functions, drag and lift were working without any modification in the code. However, due to a bug in the source code total pressure and mass flow rate could not be used as objective functions, which are much more suitable for a turbomachinery optimization study. To use these objective functions, the source code had to be altered slightly. The adaptation consisted of minor name changes. SU2 would print out total pressure and mass flow with a slightly different name in its history file and would not recognize these as the same with the corresponding objective functions, which would disrupt the optimization routine at the very first design iteration. By making these history output and objective/constraint function names consistent, total pressure and mass flow could be used as objective/constraint functions. Drag and total pressure are the two objective functions performed better compared to others and were more suitable for the optimization study. Drag is used for constraint function as to somewhat limit the shape deformation. Specifying *Drag > 0* as the constraint helps the optimizer keep shape deformations more subtle. Total pressure at the outlet is given as the main objective function. Drag direction in SU2 is determined from the freestream angle of attack. Giving a zero angle of attack for the freestream and positioning the blade exactly parallel in that direction and constraining the optimization with positive drag prevented unreasonable deformations. Curvature of the surface inside the FFD box is selected as the design variable. The deformation is done by changing the curvature of the surface that is covered in the FFD box.

The optimization is carried out for a single operating condition and that operating condition is shown in Figure 18. The point where the efficiency is the lowest is chosen as the operating point for optimization. Since this is a 3D case simplified to a 2D one, the boundary conditions are taken from the 3D case and applied to the stand alone 2D vane geometry. Due to optimization being done on a single operating point, major changes in geometry are avoided. To achieve this, only the portion where a

significant flow separation happens is chosen as the geometry portion that is to be optimized. Only the portion where flow separation is seen at the suction side of the blade is included inside the FFD box, excluding the pressure side, and leading edge and trailing edge portions of the blade. The streamlines around the vane are shown in Figure 20. The blue streamlines show the separated flow region for the selected optimization condition. Also, the FFD box used for the optimization study is shown in Figure 20 as well.

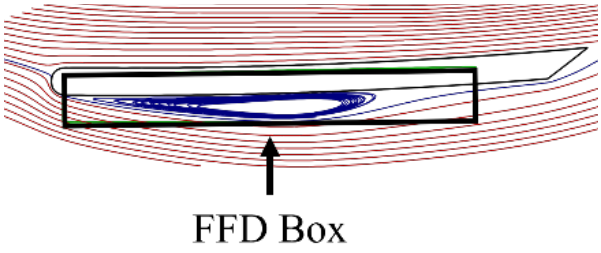

Figure 20. Streamlines Around the Diffuser Vane and the FFD Box for the Optimization Study

As for the optimization results, a total of 20 design iterations were carried out. The change in total pressure loss between inlet and outlet with each design iteration is shown in Figure 21.

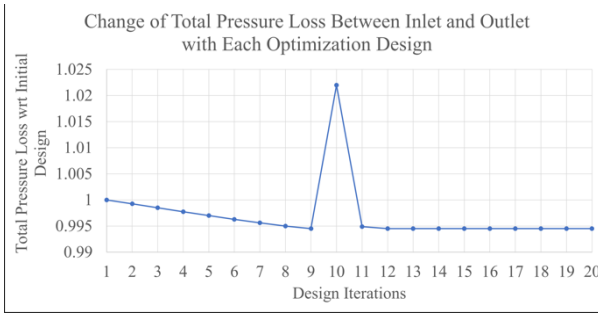

Figure 21. Change of Total Pressure Loss Between Inlet and Outlet with Each Design Iteration

As it can be seen from Figure 21, at 10th design iteration there is a jump. This is due to SU2 trying to continue changing the shape of the interested area in the same way as it was changing the shape in the previous design iterations. However, because of this, the total pressure loss between diffuser inlet and outlet increases. Thus, SU2 changes the direction it changed the shape so far for the next design iteration. After some design iterations SU2 converges to an optimum design that is very similar to 9th design iteration. This indicates that after the 9th design iteration, SU2 reached the shape deformation limit for the given objectives and constraints.

Since the optimization is done to a very small portion of the blade the change in total pressure at the outlet is very minor. However, the total pressure loss between diffuser inlet and outlet is decreased by 0.55%. Considering that this geometry was designed for an interval of operating points, the increase in total pressure for one of the worst operating points with minimal change in the geometry is expected to be small.

In Figure 22, initial and optimized blade profiles are shown, with a closeup of the most deformed area. Also, in Figure 23, Mach contour around this most deformed area is shown. With the optimized blade profile, it can be said that flow separation starting location is slightly moved downstream.

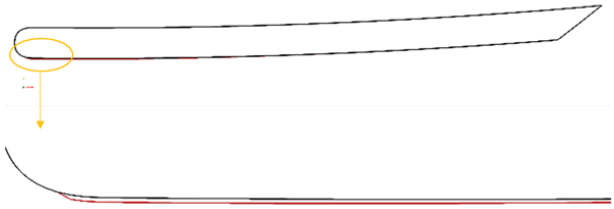

Figure 22. Initial (Black) and Optimized (Red) Vane Blade Profiles

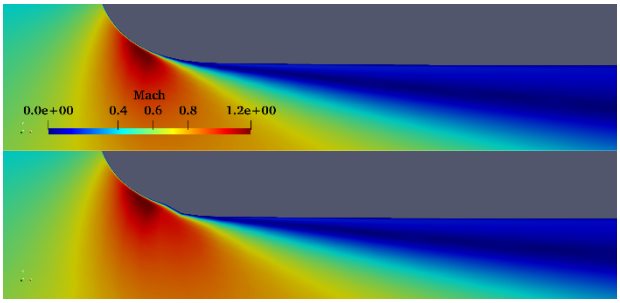

Figure 23. Mach Contour Near the Most Deformed Location, Original (Top) vs Optimized (Bottom) Profiles

Moreover, the effect of the geometry optimization on the compressor performance at the operating point with highest efficiency is also tested. When the original and optimized vane geometries are compared, it was found out that the optimized vane geometry resulted in a 0.86% increase in the total pressure loss at the vane outlet. Compared to the achieved decrease in the total pressure loss at the operating point used in the optimization study this increase seen at the operating with the highest efficiency is slightly more significant. This shows the importance of conducting optimization studies considering the entire operating curve of the compressor.

CONCLUSION

In this study the capabilities of SU2 for analyzing compressible turbomachinery flows were tested on two different centrifugal compressor geometries. The performance parameters derived from simulation results were compared against experimental data and against 'Fidelity Flow', a commercial solver for turbomachinery flows. Results showed that SU2 predicted the performance parameters of the compressors with minor differences relative to the predictions of the commercial tool. In addition to the performance parameters, the

numerical accuracy of SU2 is also tested on a more detailed flow field analysis. There, significant differences were observed between the predictions of SU2 and 'Fidelity Flow'. The first order accurate discretization scheme in space is thought of as the primary factor for the more diffused flow field solutions with SU2.

The capabilities of the adjoint optimization toolbox included in SU2 is also investigated as well. Even though it required some amount of work to obtain a functioning and meaningful optimization case setup, in the end it was possible to carry out an optimization study on the diffuser vane with SU2. The optimized vane geometry reduced the losses by 0.55% generated by the flow separation downstream of the vane leading edge. However, testing the geometry optimized for the specific operating point close to choke conditions at another operating point with the best efficiency resulted to a performance deterioration. This points out the necessity for a multi-point optimization algorithm for turbomachinery applications. Also, shape deformation tool within the optimization toolbox should be improved to increase the capability of the tool in handling geometrical discontinuities in the optimized geometry.

Additionally, SU2 has very limited turbomachinery specific post-processing capabilities. It only has two turbomachinery specific outputs, and these are kinematic and thermodynamic values at spanwise locations at the inlet and outlet of the corresponding zones. Kinematic values consist of Mach, velocity, and absolute and relative flow angles. Thermodynamic values consist of pressure, temperature, enthalpy and total counterparts of these, and density. Especially for radial turbomachinery a more extended post-processing capability that enables to generate meridional, constant angular and spanwise cut planes is a necessity.

In conclusion, SU2 is a promising open-source software for handling compressible turbomachinery flows. It works with a simple text-based input file, which makes it a user-friendly application for first-time users. Also, its turbomachinery specific settings make it more usable, especially for internal flow applications compared to other open-source alternatives. Optimization package included in SU2 is also a nice to have tool for simple optimization cases. However, it required some source code modifications to be able to use turbomachinery specific objective functions.

REFERENCES

de Castro İ.C., 2019, Assessment of SU2 for radial compressor performance prediction, [Online]. Available: http://resolver.tudelft.nl/uuid:604be835-1715-42e9-bd87-a856322f71d4

Yan C., Wang B., He X., Zhao F., Zheng X., Vahdati M. and Zheng X., 2023, Extension and Validation of the Turbomachinery Capabilites of SU2 Open-SOurce CFD Code, *Turbomachinery Technical Conference and Exposition, Boston.*

Mollá V.F., 2017, 3D-simulation of multi-stage turbomachinery by means of a non-reflecting mixing plane interface, [Online]. Available: http://resolver.tudelft.nl/uuid:324b6057-aeab-4ad8-ab24-5aa1a62819a0

Keep J.A., Vitale S., Pini M. and Burigana M., 2017, Preliminary verification of the open-source CFD solver SU2 for radial-inflow turbine applications, *Energy Procedia*, vol. 129, pp. 1071-1077.

Giles M., 1990, Nonreflecting boundary conditions for Euler equation calculations, *AIAA*, pp. 2050-2058.

de Koning R.C.V., 2015, Development of a Parametric 3D Turbomachinery Blade Modeler, [Online]. Available: http://resolver.tudelft.nl/uuid:9bbcf030-af4b-42c8-a7e5-2157bde13706

Vitale S., Pini M., Colonna P., 2020, Multistage Turbomachinery Design Using the Discrete Adjoint Method Within the Open-Source Software SU2, *Journal of Propulsion and Power*, pp. 1-14.

Rubino A., Vitale S., Colonna P., Pini M., 2020, Fully-turbulent adjoint method for the unsteady shape optimization of multi-row turbomachinery," *Aerospace Science and Technology*, vol. 106.

Giles M.B., Pierce N.A., 2000, An introduction to the Adjoint Approach to Design, *Flow, Turbulence and Combustion*, vol. 65, pp. 393-415.

Ntanakas G.D., Meyer M., 2014, Towards Unsteady Adjoint Analysis for Turbomachinery Applications, *European Conference on Computational Fluid Dynamics (ECFD VI), Barcelona.*

Katsapoxaki P., Hottois R., Tran T.S., Schram C., Coussement G., Verstraete T., 2023, Adjoint-Based Aeroacoustic Optimization of NASA Rotor 37, *Proceedings of ASME Turbo Expo 2023: Turbomachinery Technical Conference and Exposition*, Boston.

Châtel A., Verstraete T., 2022, Aerodynamic Optimization of the SRV2 Radial Compressor Using an Adjoint-Based Optimization Method, *Proceedings of ASME Turbo Expo 2022: Turbomachinery Technical Conference and Exposition*, Rotterdam.

Hottois R., Châtel A. Verstraete T., 2023, Adjoint-Based Design Optimization of a Volute for a Radial Compressor, *Int. J. Turbomach. Propuls. Power*, vol. 8, no. 4.

Trompoukis X.S., Tsiakas K.T., Asouti V.G., Giannakoglou K.C., 2023, Continuous Adjoint-Based Shape Optimization of a Turbomachinery Stage using a

3D Volumetric Parameterization, *International Journal for Numerical Methods in Fluids*, vol. 95, no. 7, pp. 1054-1075.

Luo J., Chen Z., Zheng Y., 2022, A Gradient-Based Method Assisted by Surrogate Model for Robust Optimization of Turbomachinery Blades, *Chinese Journal of Aeronautics*, vol. 35, no. 10, pp. 1-7.

Wu H., Da X., Wang D., Huang X., 2023, Multi-Row Turbomachinery Aerodynamic Design Optimization by an Efficient and Accurate Discrete Adjoint Solver, *Aerospace*, vol. 10, no. 2.

Hicks R.M., Henne P.A., 1978, Wing Design by Numerical Optimization, *J. of Aircraft*, vol. 15, no. 7.

Koshakji A., Quarteroni A., Rozza G., 2013, Free Form Deformation Techniques Applied to 3D Shape Optimization Problems, https://www.epfl.ch/labs/mathicse/wp-content/uploads/2018/10/44.2013_AK-AQ-GR.pdf .

Menter F.R., 1994, Two-equation Eddy-viscosity Turbulence Models for Engineering Applications", *AIAA*, vol. 32, no. 8, pp. 1598-1605.